

MULTIDIMENSIONAL SIMULATIONS FOR EARLY-PHASE SPECTRA OF ASPHERICAL HYPERNOVAE: SN 1998bw AND OFF-AXIS HYPERNOVAE

MASAOMI TANAKA,¹ KEIICHI MAEDA,^{2,3} PAOLO A. MAZZALI,^{1,2,4} AND KEN'ICHI NOMOTO^{1,5}

Received 2007 April 20; accepted 2007 August 22; published 2007 September 24

ABSTRACT

Early-phase optical spectra of aspherical jet-like supernovae (SNe) are presented. We focus on energetic core-collapse SNe, or hypernovae. Based on hydrodynamic and nucleosynthetic models, radiative transfer in the SN atmosphere is solved with a multidimensional Monte Carlo radiative transfer code, SAMURAI. Since the luminosity is boosted in the jet direction, the temperature there is higher than in the equatorial plane by ~ 2000 K. This causes anisotropic ionization in the ejecta. Emergent spectra are different depending on viewing angle, reflecting both aspherical abundance distribution and anisotropic ionization. Spectra computed with an aspherical explosion model with kinetic energy 20×10^{51} ergs are compatible with those of the Type Ic SN 1998bw if $\sim 10\%$ – 20% of the synthesized metals are mixed out to higher velocities. The simulations enable us to predict the properties of off-axis hypernovae. Even if an aspherical hypernova explosion is observed from the side, it should show hypernova-like spectra but with some differences in the line velocity, the width of the Fe absorptions, and the strength of the Na I line.

Subject headings: radiative transfer — supernovae: general — supernovae: individual (SN 1998bw)

1. INTRODUCTION

The connection between the long gamma-ray bursts (GRBs) and a special class of Type Ic supernovae (GRB-SNe) is now well established (Galama et al. 1998; Hjorth et al. 2003; Stanek et al. 2003; Malesani et al. 2004; Pian et al. 2006). Since GRBs are induced by relativistic jets, GRB-SNe are also expected to be aspherical. There is also increasing evidence that core-collapse SNe are not spherically symmetric, coming from, e.g., the detection of polarization in several SNe (e.g., Wang et al. 2001; Kawabata et al. 2002; Leonard et al. 2006) and late-time spectroscopy (Mazzali et al. 2005).

However, the progenitors, the explosion mechanisms, and the origins of diverse properties of GRB-SNe are still not understood (e.g., Nomoto et al. 2007). In order to answer such questions, it is crucial that the properties of the explosions (e.g., the mass and kinetic energy of the ejecta and the asymmetry of the explosion) are accurately derived from observations. For this purpose, we should know the observational properties of multidimensional SN explosions and to what degree they are affected by orientation effects.

This is an area that has not been studied in great depth, despite its importance. Although some works have addressed the properties of the light curve (LC) or the late-phase spectra of aspherical SNe (e.g., Höflich et al. 1999; Maeda et al. 2002, 2006a, 2006b; Sim 2007), only a few studies of early-phase spectra ($t \lesssim 50$ days, where t is the time since the explosion) have been performed (e.g., Höflich et al. 1996 for core-collapse SNe; Thomas et al. 2002; Kasen et al. 2004; Tanaka et al. 2006 for Type Ia SNe).

SNe that associate with GRBs are thought to be highly energetic explosions, i.e., hypernovae (here defined as SNe with ejecta kinetic energy $E_{51} = E_K/10^{51}$ ergs > 10 ; e.g., Nomoto et al. 2006) indicated by broad line features in their early-phase spectra. However,

this suggestion was based on analyses that assumed spherical symmetry. No realistic multidimensional explosion models have been verified against the observed early-phase spectra.

We report the first study of early-phase spectra of aspherical hypernova models using a multidimensional radiative transfer code. The synthetic spectra are compared with observed spectra of SN 1998bw, and implications for off-axis hypernovae are discussed.

2. MODELS

We use the results of multidimensional hydrodynamic and nucleosynthetic calculations for SN 1998bw (Maeda et al. 2002) as input density and element distributions. In the present simulations, 16 elements are included, i.e., H, He, C, N, O, Na, Mg, Si, S, Ti, Cr, Ca, Fe, Co, and Ni. Since the original models used a He star as a progenitor, we simply replace the abundance of the He layer with that of the C+O layer. In the hydrodynamic model, energy is deposited aspherically, with more energy in the jet direction (z -axis). As a result, ^{56}Ni is preferentially synthesized along this direction (see Fig. 3 of Maeda et al. 2002). In this Letter, an aspherical model with $E_{51} = 20$ (A20) and two spherical models with $E_{51} = 20$ and 50 (F20 and F50, respectively) are studied (Table 1). They are constructed on the basis of the models with $E_{51} = 10$ (Maeda et al. 2002, 2006a).

Bolometric LCs computed in three-dimensional space by Maeda et al. (2006a) are also used as input for the spectral calculations. A common problem in modeling hypernova LCs is that a spherical model reproducing the early rise of the LC ($E_{51} = 50$ for SN 1998bw) declines more rapidly than the observed LC at $t \sim 100$ – 150 days (Nakamura et al. 2001; Maeda et al. 2003). This problem can be solved by aspherical models with a polar view. In aspherical models, even with a lower kinetic energy ($E_{51} = 10$ – 20) than in the spherical case ($E_{51} = 50$), which allows sufficient trapping of γ -rays at late times, the rapid rise of the LC can be reproduced because of the extended ^{56}Ni distribution (Maeda et al. 2006a).

3. METHOD

In order to study the detailed properties of the radiation from aspherical SNe, we have unified a Supernova MULTIdimensional RAdiative transfer code (SAMURAI). SAMURAI is a combination

¹ Department of Astronomy, Graduate School of Science, University of Tokyo, Tokyo, Japan; mtanaka@astron.s.u-tokyo.ac.jp.

² Max-Planck-Institut für Astrophysik, Garching bei München, Germany; maeda@mpa-garching.mpg.de.

³ Department of Earth Science and Astronomy, Graduate School of Arts and Science, University of Tokyo, Tokyo, Japan.

⁴ Istituto Nazionale di Astrofisica, OATs, Trieste, Italy.

⁵ Institute for the Physics and Mathematics of the Universe, University of Tokyo, Kashiwa, Japan.

TABLE 1
SUMMARY OF EXPLOSION MODELS

Model Name	M_{ej}^a	E_{51}	$M(^{56}\text{Ni})^b$	p^c
A20	10	20	0.39	0.0
F20	10	20	0.31	0.0
F50	10	50	0.40	0.0
A20p0.2	10	20	0.39	0.2

^a The mass of the ejecta (M_{\odot}).

^b The ejected ^{56}Ni mass (M_{\odot}).

^c The mixing fraction (see § 5).

of three-dimensional codes adopting Monte Carlo methods to compute the bolometric LC (Maeda et al. 2006a) and the spectra of SNe from early (Tanaka et al. 2006) to late (Maeda et al. 2006b) phases. The LCs are computed as pioneered by Cappellaro et al. (1997). Our three-dimensional LC code adopts the individual packet method as described by Lucy (2005) and in addition includes multi-energy transfer for high-energy photons (Maeda 2006).

The early-phase spectra are calculated as snapshots in the optically thin atmosphere, using the results of the LC simulation as initial conditions. A sharply defined photosphere is assumed as an inner boundary for simplicity. The position of the inner boundary in each direction is determined by averaging the positions of the last scattering photon packets (see Fig. 3 of Maeda et al. 2006a). Thus, the inner boundary corresponds to an optical depth of roughly unity. The luminosity at the inner boundary [$L_{\text{in}}(\theta)$] is also taken from the LC computation by integrating the energy of photon packets escaping from each θ bin.

For the computation of ionization and excitation state in the atmosphere, the local physical process the same as in the previous one-dimensional code (Mazzali & Lucy 1993; Mazzali 2000), which is used to model spectra of SNe of various types (e.g., Mazzali et al. 1993), is adopted. Line scattering under the Sobolev approximation and electron scattering are taken into account. For line scattering, the effect of photon branching is included as in Lucy (1999). Beginning with a trial temperature structure, a number of photon packets (typically $\sim 10^8$ – 10^9) are followed in three-dimensional space, giving the flux in each mesh. Then the temperature structure is updated. After the temperature structure converges, the spectra are obtained by counting the energy (or wavelength) distribution of escaping photon packets in every direction.

Since the background model is axially symmetric, it is not necessary to follow the propagation in the azimuthal direction explicitly. We use a two-dimensional grid (r, θ) but still perform the transport of the photon packets in three dimensions, reproducing photon propagation in the azimuthal direction by projecting the photon back on the two-dimensional plane of the calculation. The spatial grid has a typical mesh number (n_r, n_{θ}) = (20, 80). Velocity is used as a proxy for the radial coordinate thanks to the homologous expansion of SN ejecta ($r = vt$). Details of the code will be presented elsewhere.

4. RESULTS

At $t = 20$ days, the photosphere of model A20 is mildly aspherical with an axis ratio of 1.4 between the polar and equatorial directions. The emergent luminosity is also anisotropic, being brighter by a factor of 1.2 in the polar direction (Maeda et al. 2006a). In contrast, the local luminosity at the photosphere, $L_{\text{in}}(\theta)$, is highly aspherical, with an axis ratio of 6.3, tracing the aspherical ^{56}Ni distribution. At this epoch, the photosphere is still outside the region where explosive nucleo-

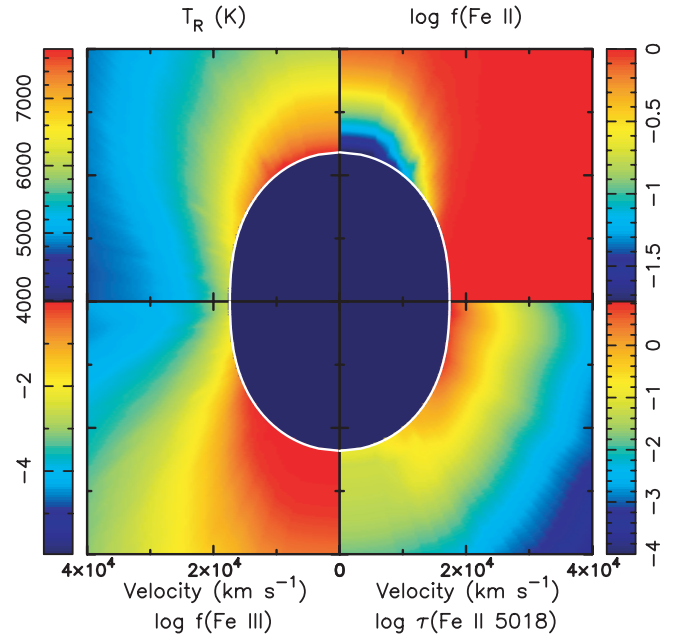


FIG. 1.—Upper left panel: Computed temperature structure in the atmosphere of model A20 at 20 days after the explosion. Upper right, lower left panels: Ionization fractions of Fe II and Fe III. Lower right panel: Sobolev optical depth of Fe II $\lambda 5018$. The vertical axis (z -axis) is the jet direction.

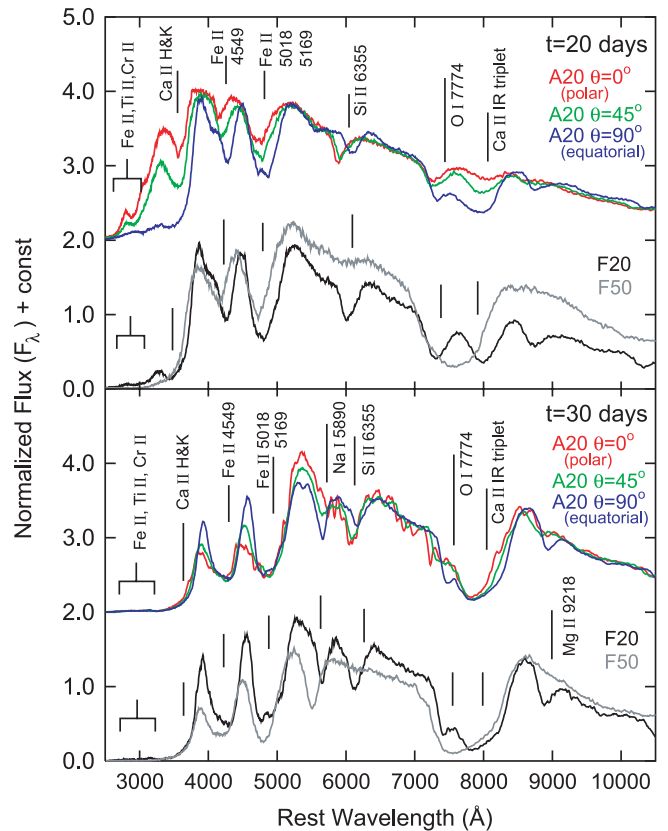


FIG. 2.—Upper panel: Synthetic spectra of model A20, F20 (black), and F50 (gray) at 20 days after the explosion. The red, green and blue lines show the spectra of model A20 seen from $\theta = 0^\circ$, 45° , and 90° , respectively. Here θ is measured from the z -axis (jet direction). Lower panel: Same as the upper panel but at 30 days after the explosion.

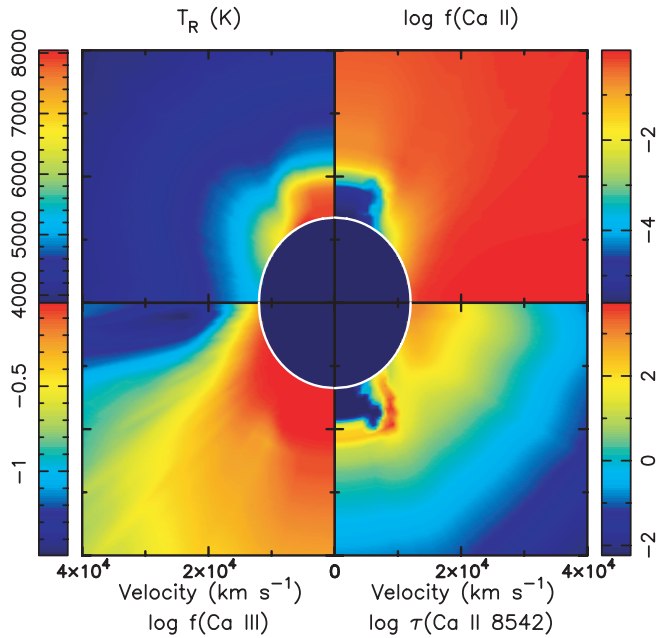


FIG. 3.—Upper left panel: Computed temperature structure in the atmosphere of model A20 at 30 days after the explosion. Upper right, lower left panels: Ionization fractions of Ca II and Ca III. Lower right panel: Sobolev optical depth of Ca II λ 8542.

synthesis occurs. The metal lines in the spectrum result from preexplosion abundance in the C+O layer.

The upper left panel of Figure 1 shows the calculated temperature structure. The boosted luminosity makes the temperature near the z -axis higher than in the equatorial plane by ~ 2000 K. This anisotropy of the temperature causes anisotropies of the ionization structure. The upper right and lower left panels of Figure 1 show the ionization fractions of Fe II and Fe III, respectively. Because of the high temperature, Fe II is suppressed by a factor of more than 30 near the z -axis. As a result, the optical depth of the Fe II lines is larger in the equatorial plane (Fig. 1, lower right panel).

The upper panel of Figure 2 shows the synthetic spectra at $t = 20$ days for models A20 (red, green, and blue: $\theta = 0^\circ$ [polar], 45° , and 90° [equatorial], respectively), F20 (black), and F50 (gray). Here θ is measured from the z -axis. All absorption lines except for Si II λ 6355 are stronger for larger θ , i.e., for an equatorial view. This is because all species that have strong lines, i.e., O I, Si II, Ca II, Ti II, Cr II, and Fe II, dominate near the equator but not near the z -axis as shown in Figure 1 for the case of Fe.⁶ This also leads to a more effective flux-blocking in the near-UV in the side-viewed spectrum.

The lower panel of Figure 2 shows the synthetic spectra at $t = 30$ days. At this epoch, the local luminosity and the temperature structure are still anisotropic, although the photosphere is almost spherical (Fig. 3, upper left panel). Consequently, the distribution of ionization fractions is also aspherical (see Fig. 3, upper right and lower left panels, for the case of Ca). However, the emergent spectra are not significantly different for different viewing angles (Fig. 2). This is the effect of the aspherical abundance distribution. The photosphere at this epoch is located inside the region where heavy elements are synthesized in the explosion. Since nucleosynthesis occurs entirely near the polar direc-

⁶ Si II λ 6355 is not strong at $\theta = 90^\circ$ because the temperature in the equatorial plane is too low to activate the transition.

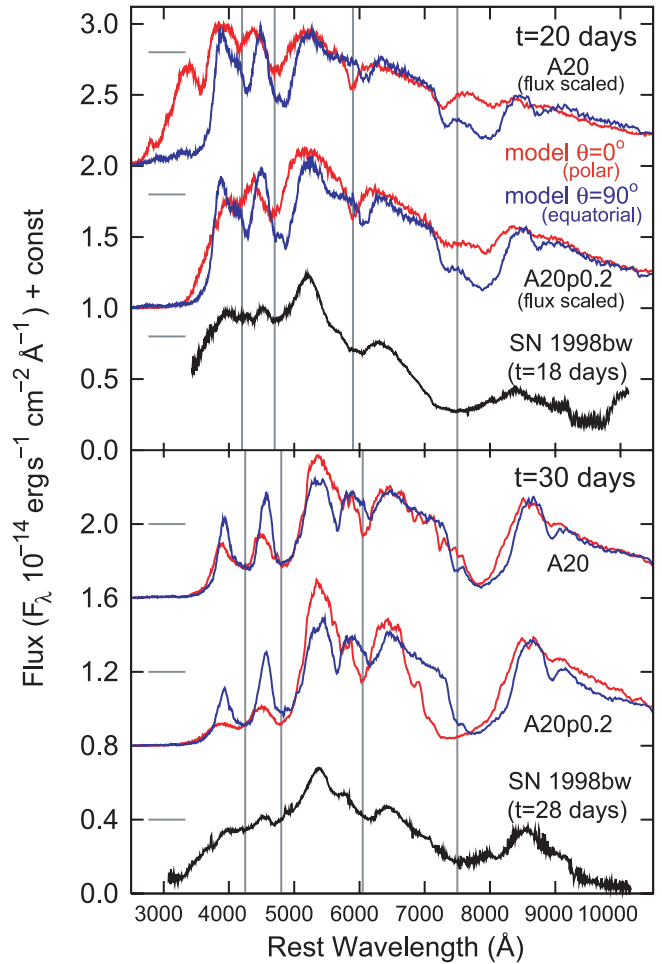


FIG. 4.—Spectra computed with model A20 and A20p.2 compared with the spectra of SN 1998bw. The synthetic spectra are reddened with $E(B - V) = 0.032$ and scaled assuming $\mu = 32.76$. Upper panel: Synthetic spectra at 20 days after the explosion (shifted upward by 2.0 and 1.0×10^{-14} , respectively) and the spectrum of SN 1998bw 18 days after GRB 980425. The flux is reduced by a factor of 1.25 after the computation. The vertical lines are drawn at 4200, 4700, 5900, and 7500 Å. The horizontal lines show the same flux level (8.0×10^{-15}). Lower panel: Synthetic spectra at 30 days after the explosion (shifted upward by 1.6 and 0.8×10^{-14} , respectively) and SN 1998bw 28 days after GRB 980425. The vertical lines are drawn at 4250, 4800, 6050, and 7500 Å. The horizontal lines show the same flux level (4.0×10^{-15}).

tion in our model, the suppression of important ions near the z -axis is compensated by the larger abundance of the heavy elements (Fig. 3, lower right panel).⁷ Only the Na I λ 5890 line is stronger for larger θ because of the combined effect of the lower temperature that favors Na I and the higher abundance of Na, which is predominantly synthesized before the explosion.

Given the strong anisotropy in $L_{\text{in}}(\theta)$, the side-viewed spectrum of model A20 consists mainly of photons escaping from the ejecta of $\theta \sim 60^\circ$. Since physical quantities there [e.g., isotropic mass and kinetic energy of the ejecta in that direction, and $L_{\text{in}}(\theta)$] are similar to those of model F20, the spectrum of model F20 is similar to the polar-viewed spectrum of model A20. Model F50 shows a very strong Na I λ 5890 line owing to the low temperature.

⁷ The Fe II absorptions are broader at $t = 30$ days than at $t = 20$ days because of more efficient absorption both near the photosphere ($v \sim 12,000$ km s^{-1} , a lower velocity than at $t = 20$ days) and at high velocity ($v \sim 25,000$ km s^{-1} , where the temperature is lower and the Fe II fraction is higher than at $t = 20$ days).

5. COMPARISON WITH SN 1998bw

The spectra computed for the aspherical model A20 are compared with those of SN 1998bw in Figure 4. Because of the detection of GRB 980425, it is tempting to compare the polar-viewed spectrum (*red lines*) with that of SN 1998bw. Since the computed LC is brighter than the observation by a factor of 1.25 at $t = 20$ days (Maeda et al. 2006a), the synthetic spectra at $t = 20$ days are scaled *after* the computation by this factor in Figure 4.

At $t = 20$ days (Fig. 4, *upper panel*), the scaled synthetic spectrum of model A20 with $\theta = 0^\circ$ does not show the broad absorption trough between 4000 and 5000 Å that is typical of hypernovae such as SN 1998bw. This is because in the model Fe line absorption is not effective at high velocities, making it possible for photons to escape effectively at 4000–5000 Å. Similarly, the O I–Ca II absorption at 7000–8000 Å is very weak in model A20. The Si line velocity in the model is, however, comparable to that in SN 1998bw.

At $t = 30$ days (Fig. 4, *lower panel*), the Ca II and Fe II lines are somewhat stronger, although the O I–Ca II absorption at 7000–8000 Å is still narrower than in the observed spectrum. The peaks around 4000 and 4500 Å are partially suppressed for a polar view by the high-velocity absorption by the extended Fe near the jet, while they are strong in the synthetic spectrum for the equatorial view. The suppression of the peaks is similarly seen in the spectrum of SN 1998bw. The Na I $\lambda 5890$ line is very weak in SN 1998bw, in analogy with the spectrum with $\theta = 0^\circ$.

The strengths of the Ca II and Fe II lines at $t = 20$ days can be increased if heavy elements synthesized in the explosion are mixed to outer layers. In SN explosions, Rayleigh-Taylor (R-T) instabilities are expected to occur,⁸ which could deliver the newly synthesized elements to higher velocities. We simulate this possibility by introducing a parameter, the mixing fraction p . If the mass ejected inside a conical section of the ejecta is $M_{ej}(\theta)$, and $M_i(\theta)$ is the mass of a certain element contained in the conical section, we simulate mixing by taking a fraction (p) of the mass of a newly synthesized element and distributing this mass homogeneously in the conical section. Thus, in the outer layers, the newly synthesized element will have an abundance $X_i(r, \theta) = pM_i(\theta)/M_{ej}(\theta)$ (plus pre-SN abundance). In the deeper region, the abundances are redistributed by a mixing down of the unburned material.

In Figure 4, synthetic spectra of models with $p = 0.2$ (model A20p0.2) are shown. At $t = 20$ days (the synthetic spectra are

similarly scaled; upper panel of Fig. 4), although the absorption line at 7000–8000 Å is still weaker than the observation, the Fe lines are strong, causing the broad absorption at $\lesssim 5000$ Å followed by the peak at ~ 5200 Å. At $t = 30$ days, the strong Ca II feature contributes to the broad absorption at 7000–8000 Å, which is comparable to that in SN 1998bw.

Although the agreement of the spectra is far from perfect, the spectra of the model with mixing are in qualitative agreement with those of SN 1998bw. Since we use multidimensional hydrodynamic and nucleosynthetic models, which are computed *ab initio*, there are not many parameters that we can freely control. The agreement could be improved by additional modifications, but they would be complicated and are beyond the scope of this work. Note that our input luminosity is higher than that of SN 1998bw at $t = 20$ days, making the ejecta temperature too high. If a luminosity comparable to that of SN 1998bw is used, neglecting the possible displacement of the photosphere, the O I–Ca II feature becomes as strong as the observation. Even in this case, however, mixing with $p \sim 0.1$ is still required.

6. CONCLUSIONS

We have presented the first detailed simulations of the early-phase optical spectra of realistic jet-like hypernova models. The emergent spectrum is different for different viewing angles. The spectral properties are determined by the combination of aspherical abundances and anisotropic ionization states.

Considering the complexity of the problem, the synthetic polar-viewed spectra are in reasonable agreement with those of SN 1998bw, when $\sim 10\%$ – 20% of the synthesized material is mixed out to higher velocities. The kinetic energy of an aspherical model that reproduces, at least qualitatively, the spectra of SN 1998bw ($E_{51} = 20$) can be smaller than that of a well-fitting spherical model ($E_{51} = 50$). This is consistent with previous results obtained from models of the LC and the late-time spectra (Maeda et al. 2006a, 2006b).

The simulations enable us to predict the properties of the early-phase spectra of hypernovae viewed off-axis. Compared with the spectra seen from the polar direction (*red*), the spectra seen from the equatorial direction (*blue*) have (1) a slightly lower absorption velocity, (2) stronger peaks around 4000 and 4500 Å, and (3) a stronger Na I $\lambda 5890$ line than in SN 1998bw. SNe similar to SN 1998bw in ejecta mass, kinetic energy, and ^{56}Ni mass should always show spectral features of “hypernovae” or “broad-line supernovae” but with some differences as described above, depending on the viewing angle.

REFERENCES

- Cappellaro, E., et al. 1997, *A&A*, 328, 203
Galama, T. J., et al. 1998, *Nature*, 395, 670
Hjorth, J., et al. 2003, *Nature*, 423, 847
Höflich, P., Wheeler, J. C., & Wang, L. 1999, *ApJ*, 521, 179
Höflich, P., et al. 1996, *ApJ*, 459, 307
Kasen, D., et al. 2004, *ApJ*, 610, 876
Kawabata, K. S., et al. 2002, *ApJ*, 580, L39
Kifonidis, K., et al. 2000, *ApJ*, 531, L123
Leonard, D. C., et al. 2006, *Nature*, 440, 505
Lucy, L. B. 1999, *A&A*, 345, 211
———. 2005, *A&A*, 429, 19
Maeda, K. 2006, *ApJ*, 644, 385
Maeda, K., Mazzali, P. A., Deng, J., Nomoto, K., Yoshii, Y., Tomita, H., & Kobayashi, Y. 2003, *ApJ*, 593, 931
Maeda, K., Mazzali, P. A., & Nomoto, K. 2006a, *ApJ*, 645, 1331
Maeda, K., Nakamura, T., Nomoto, K., Mazzali, P. A., Patat, F., & Hachisu, I. 2002, *ApJ*, 565, 405
Maeda, K., Nomoto, K., Mazzali, P. A., & Deng, J. 2006b, *ApJ*, 640, 854
Malesani, J., et al. 2004, *ApJ*, 609, L5
Mazzali, P. A. 2000, *A&A*, 363, 705
Mazzali, P. A., & Lucy, L. B. 1993, *A&A*, 279, 447
Mazzali, P. A., et al. 1993, *A&A*, 269, 423
———. 2005, *Science*, 308, 1284
Nakamura, T., et al. 2001, *ApJ*, 550, 991
Nomoto, K., et al. 2006, *Nucl. Phys. A*, 777, 424
———. 2007, *Nuovo Cimento*, 121, 1207
Pian, E., et al. 2006, *Nature*, 442, 1011
Sim, S. A. 2007, *MNRAS*, 375, 154
Stanek, K. Z., et al. 2003, *ApJ*, 591, L17
Tanaka, M., et al. 2006, *ApJ*, 645, 470
Thomas, R. C., et al. 2002, *ApJ*, 567, 1037
Wang, L., et al. 2001, *ApJ*, 550, 1030